Synthesis and Photovoltaic Properties of a Solution-Processable Organic Molecule Containing Triphenylamine and DCM Moieties

Chang He,[†,§] Qingguo He,[†] Xiaodi Yang,[†,§] Guanglong Wu,[†,§] Chunhe Yang,[†] Fenglian Bai,*[,†] Zhigang Shuai,[†] Lingxuan Wang,[‡] and Yongfang Li*[,†]

Beijing National Laboratory for Molecular Sciences, CAS Key Laboratory of Organic Solids, Institute of Chemistry, Chinese Academy of Sciences, Beijing 100080, China, CAS Key Laboratory of Photochemistry, Institute of Chemistry, Chinese Academy of Sciences, Beijing 100080, China, and Graduate University of Chinese Academy of Sciences, Beijing 100039, China

Received: January 27, 2007; In Final Form: April 26, 2007

A solution processible organic conjugated molecule 2-[2,6-bis-(2-{4-[2-(4-diphenylaminophenyl)vinyl]phenyl}-vinyl)pyran-4-ylidene]malononitrile (TPA−DCM−TPA) was designed and synthesized for application in organic solar cells (OSCs). The molecule consists of two electron-rich triphenylamine moieties and one electron-deficient 2-pyran-4-ylidenemalononitrile unit linked with conjugated bridges. The optical and electrochemical properties, the light-induced electron spin resonance (LESR), and the electronic ground state configuration of the compound were characterized. TPA−DCM−TPA film showed a broad absorption band covering from 350 to 650 nm. The bulk-heterojunction OSCs with the device structure of ITO/PEDOT:PSS/TPA−DCM−TPA:PCBM/LiF/Al or Ba/Al were fabricated, in which TPA−DCM−TPA was used as donor and PCBM as acceptor material. The open-circuit voltage, short-circuit current, and power-conversion efficiency of the optimized OSC with Ba/Al as cathode, TPA−DCM−TPA:PCBM = 1:3 (w/w), and ca. 85 nm thickness of the active layer reached 0.9 V, 2.14 mA/cm^2, and 0.79%, respectively, under the illumination of AM1.5, 100 mW/cm^2. The results indicate that TPA−DCM−TPA is a promising photovoltaic organic molecule.

1. Introduction

Organic and polymer solar cells have attracted great attention in recent years because of the importance of utilizing solar energy and their advantages of easy fabrication, low cost, and light weight in comparison with their inorganic counterpart.[1−7] Currently, the power-conversion efficiencies (η) of both polymer solar cells (PSCs) with spin-coating bulk-heterojunction structure[8,9] and organic small-molecule solar cells (OSCs) with vacuum-evaporating interpenetrating bilayer structure[10,11] have already attained 5%, which is the threshold value for possible commercial applications.

The preparation technique of the organic active layer in fabricating the devices and the visible absorption characteristics of the organic materials are two important aspects which should be taken into account in the selection of the organic photovoltaic materials. The cost of device fabrication is a vital factor that influences the commercial applications. For the preparation of the photosensitive layers of solar cells, spin-coating has been demonstrated to be an easy and low-cost fabrication process in comparison with vacuum evaporation.[12−14] Therefore, the solution processability of the organic and polymer photovoltaic materials is a very important factor for the low-cost fabrication of devices.

Most of the photovoltaic conjugated polymers have the advantage of solution processability. However, the purification of polymers is difficult, and they are the mixture of the polymer molecules with different molecular weights. In fact, both the purity of the photovoltaic materials[15] and the molecular weights of the conjugated polymers[16] strongly affected the device performance. In contrast with polymers, organic small molecules have well-defined molecular structures and definite molecular weights without any distribution, and their purity can be strictly controlled. Therefore, the organic small molecules with good solution-processability and effective absorption of sunlight could be promising photovoltaic materials.

Organic small molecules usually are easy to crystallize and, thus, are difficult to form a uniform film by the solution-processing method. It was found that adding nonplanar moiety in the molecules could improve their solution-processability,[17,18] and the strategy has been used in the design of organic electroluminescent materials.[19] Therefore, triphenylamine (TPA) moiety with three-dimensional propeller structure is a suitable component unit to reach the solution-processability.

The utility of the sunlight is, of course, a key issue for the organic photovoltaic materials. Hence, strong and broad absorption in the visible and near-infrared region is desirable for the organic molecules used in the OSCs. For enhancing the absorption of the materials, Roncali proposed the following molecular design principles: (1) connecting the electron-donor and electron-acceptor moieties via conjugated bridge and (2) adjusting the ability of pull−push electrons of the acceptor and donor moieties to control the electronic energy levels of the molecules.[20−22] Considerable research efforts have led to major progress in the synthesis of new molecules. Their chemical structures mainly consist of a TPA moiety linked to different acceptor moieties, including indanedione or dicyanovinyl,[23] perylene,[24] and thiadiazole,[25] as well as X-shaped oligothiophenes.[26] Under the condition of AM1.5, 100 mW/cm^2, the

* Corresponding author. E-mail: liyf@iccas.ac.cn. Tel.: 86-10-62536989.
† CAS Key Laboratory of Organic Solids, Institute of Chemistry, Chinese Academy of Sciences.
‡ CAS Key Laboratory of Photochemistry, Institute of Chemistry, Chinese Academy of Sciences.
§ Graduate University of Chinese Academy of Sciences.

10.1021/jp070714x CCC: $37.00
Published on Web 05/27/2007

SCHEME 1: Synthesis Route of TPA−DCM−TPA

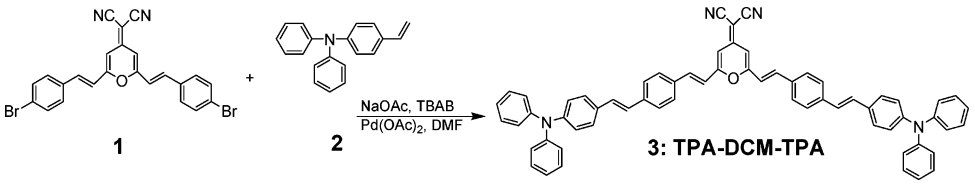

maximum power-conversion efficiency of the bulk-heterojunction OSC based on the above materials reported so far is 0.81%.[23] In the molecules, triphenylamine moiety is an electron-rich unity as well as the moiety to improve the solution-processability for the application in OSC devices.

In this paper, we designed and synthesized a new solution-processable and TPA-containing molecule 2-[2,6-bis-2-{4-[2-(4-diphenylaminophenyl)vinyl]phenyl}vinyl]pyran-4-ylidene]-malononitrile (TPA−DCM−TPA) for the application in OSCs. The molecular structure of TPA−DCM−TPA is shown as compound **3** in Scheme 1. The consideration of the molecular design of TPA−DCM−TPA is that the spatially nonplanar TPA is used as the electron-rich moiety, and the dye 2-pyran-4-ylidenemalononitrile (PM) is used as the electron-deficient moiety for getting broad absorption and suitable electronic energy levels. TPA−DCM−TPA film showed a broad absorption band covering from 350 to 650 nm. The bulk-heterojunction OSCs were fabricated by spin-coating the blend solution of TPA−DCM−TPA as donor and [6,6]-phenyl C_{61}-butyric acid methyl ester (PCBM) as acceptor material. The open-circuit voltage (V_{oc}), short-circuit current (I_{sc}), and power-conversion efficiency (η) of the OSC device reached 0.9 V, 2.14 mA/cm^2, and 0.79%, respectively, under the illumination of AM1.5, 100 mW/cm^2. The efficiency of 0.79% is one of the best values reported so far for the OSCs based on the solution-processable organic small molecules.

2. Experimental Section

2.1. Materials. All chemicals were purchased from Aldrich or Acros chemical Co. and were used without any further purification, except that DMF was freshly distilled prior to use and PCBM was purchased from ADS Company (purity > 99.9%).

2.2. Synthesis of TPA−DCM−TPA. TPA−DCM−TPA was synthesized by the Heck reaction with the synthesis route shown in Scheme 1. 2-{2,6-bis-[2-(4-Bromophenyl)vinyl]pyran-4-ylidene}malononitrile (**1**)[27] and biphenyl-(4-vinylphenyl)amine (**2**)[28] were synthesized according to the procedures described in the literature. Under argon flow, 0.506 g (1 mmol) of compound **1**, 0.5427 g (2 mmol) of compound **2**, 11.22 mg of Pd $(OAc)_2$, 64.47 mg of *n*-Bu_4NBr, and 0.43 g (5.2 mmol) of NaOAc were added to a two-necked flask with condenser, balloon, and septum, and then 20 mL of degassed dimethylformamide (DMF) was injected by syringe. The above mixture solution was heated to 100 °C and kept at that temperature until the disappearance of compound **2** monitored by thin-layer chromatography (TLC). Then the solution was cooled to room temperature and poured into distilled water. The precipitate was filtered, washed with water, dissolved in methylene chloride, and dried over $MgSO_4$. After column separation (SiO_2, petroleum ether/methane chloride 1:1), 479 mg of dark reddish brown powder of TPA−DCM−TPA was obtained with a yield of 54.1%. ^{1}H NMR (400 MHz, $CDCl_3$, δ/ppm): 7.56 (s, 2H, Ar−H), 7.03 (m, 30H, N−Ph−H), 7.11 (d, 4H, Ph−H), 7.27 (d, 4H, Ph−H), 6.07 (m, 4H). MALDI-TOF-MS confirmed the chemical structure of TPA−DCM−TPA (*m*/*z*): 886.4, calcd for $C_{64}H_{46}N_4O$, 886.37.

2.3. Instruments and Measurements. ^{1}H NMR spectra were measured on a Bruker DMX-400 spectrometer. Absorption and photoluminescence (PL) spectra were taken on a Hitachi U-3010 UV−vis spectrophotometer and Hitachi F-4500 spectrophotometer, respectively. The electrochemical cyclic voltammetry was conducted on a Zahner IM6e electrochemical workstation. A glassy carbon coated with the sample film was used as the working electrode; a Pt wire and a Ag wire were used as counterelectrode and reference electrode, respectively. The electrode potential of the Ag wire quasi-reference electrode was calibrated with saturated calomel electrode (SCE), and it is −0.1 V vs SCE. The light-induced electron spin resonance (LESR) experiments were carried out using a Bruker E500 with field-modulation amplitude of 3.0×10^{-4} T, microwave frequency of 9.65×10^9 Hz, and microwave power of 2 mW, at 300 K. The LESR experimental procedure consisted of the following sequence: (1) scanning the ESR spectrum of the nonilluminated sample; (2) scanning the ESR spectrum of the illuminated sample; and (3) turning off the illumination and scanning the ESR spectrum of the sample again. An Ar^+-ion laser at 500 nm was used for light excitation.

2.4. Fabrication and Characterization of OSC Devices. The organic solar cells were fabricated in the configuration of the traditional sandwich structure with indium tin oxide (ITO) glass anode and metal cathode. Patterned ITO glass with a sheet resistance of 30 Ω/□ was purchased from CSG Holding Co., Ltd. (China). The ITO glass was cleaned in an ultrasonic bath of acetone and isopropanol, and then it was treated in an ultraviolet-ozone chamber for 0.5 h (Ultraviolet Ozone Cleaner, Jelight Company, U.S.A.). Then a thin layer (30 nm) of PEDOT:PSS (poly(3,4-ethylenedioxythiophene)−poly(styrene sulfonate)) (Baytron PVP A1 4083 Germany) was spin-coated on the ITO glass and baked at 150 °C for 0.5 h. Subsequently, the photosensitive active layer was prepared by spin-coating the toluene solution of TPA−DCM−TPA or the blend chlorobenzene solution of TPA−DCM−TPA and PCBM with different weight ratios (2:1, 1:1, 1:2, 1:3, 1:4 w/w) on the top of the PEDOT:PSS layer. The thickness of the active layers was measured by Ambios Technology XP-2 profilometer. A thin layer of LiF (0.8 nm) or barium (10 nm) was evaporated before aluminum evaporation. The thermal evaporation was done under a shadow mask in a base pressure of ca. 10^{-4} Pa. The active area of a device was 4−6 mm^2. The current−voltage (I−V) measurement of the devices was conducted on a computer-controlled Keithley 236 Source measure unit. A xenon lamp coupled with AM1.5 solar spectrum filters was used as the light source, and the optical power at the sample was around 100 mW/cm^2. The input photon to converted current efficiency (IPCE) was measured using a Keithley 2000 System DMM coupled with WDG3 monochromator and 500 W xenon lamp. The light intensity at each wavelength was calibrated with a standard single-crystal Si photovoltaic cell. The atomic force microscopy (AFM) measurement of the surface morphology of

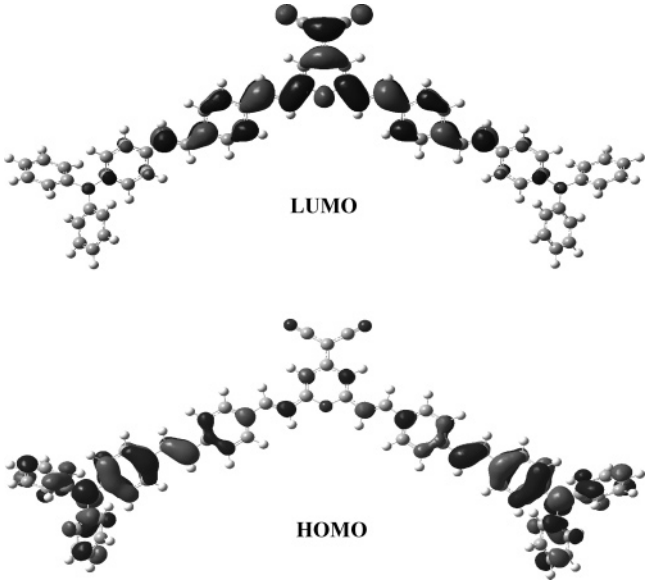

Figure 1. Molecular orbital surfaces of the HOMO and LUMO of TPA−DCM−TPA obtained at B3 LYP/6-31G* level.

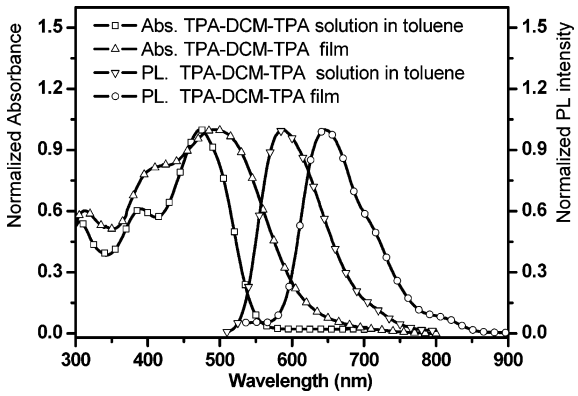

Figure 2. UV−vis absorption and photoluminescence (PL) spectra of TPA−DCM−TPA in toluene solution and in film state.

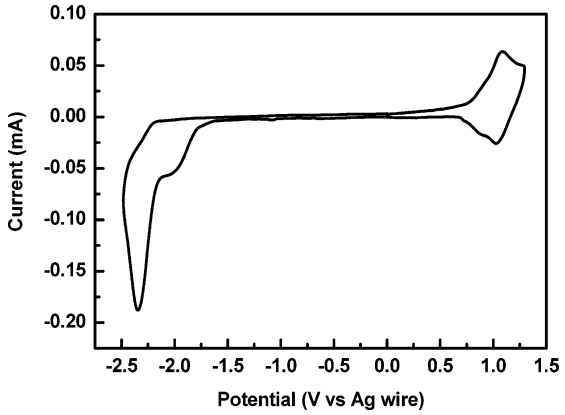

Figure 3. Cyclic voltammograms of TPA−DCM−TPA film on glassy carbon electrode in an acetonitrile solution of 0.1 mol/L Bu_4NPF_6 (Bu = butyl) with a scan rate of 20 mV/s.

samples was conducted on a Nanoscope III (DI, U.S.A.) in contacting mode with 1 or 5 μm scanners.

3. Results and Discussion

3.1. Molecular Structure and Properties. The optimum geometry and electron-state-density distribution of the highest occupied molecular orbital (HOMO) and the lowest unoccupied molecular orbital (LUMO) of TPA−DCM−TPA were calculated by the quantum-chemical Hartree−Fock method with configure interaction singlet excited state (CIS). A split-valence double-ζ basis set, 6-31G+**, was adopted in the calculation. Figure 1 shows the optimum geometry and the electron-state-density distribution of the HOMO and LUMO of the TPA−DCM−TPA molecule. The HOMO state density mainly distributed on the two triphenylamine (TPA) moieties with some extending to the two phenyl units of the molecule. The electron density of LUMO was mainly localized at the 2-pyran-4-ylidenemalononitrile (PM) moiety. Besides, the optimized geometry of TPA−DCM−TPA indicates that the two TPA moieties at the end of the molecule are in 3-D spatial arrangement, which makes the molecular structure nonplanar. The nonplanar molecular structure of TPA−DCM−TPA could be beneficial to solution-processability to form amorphous film.

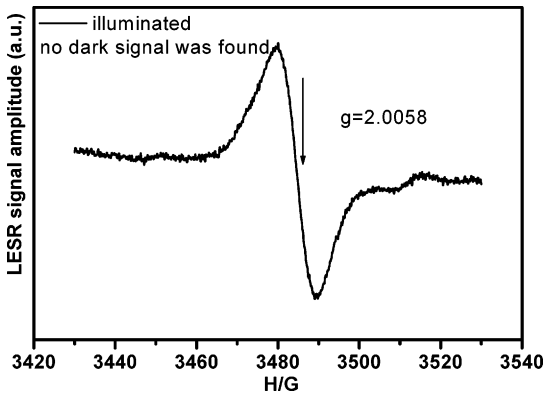

Figure 4. Light-induced electron spin resonance spectrum of TPA−DCM−TPA.

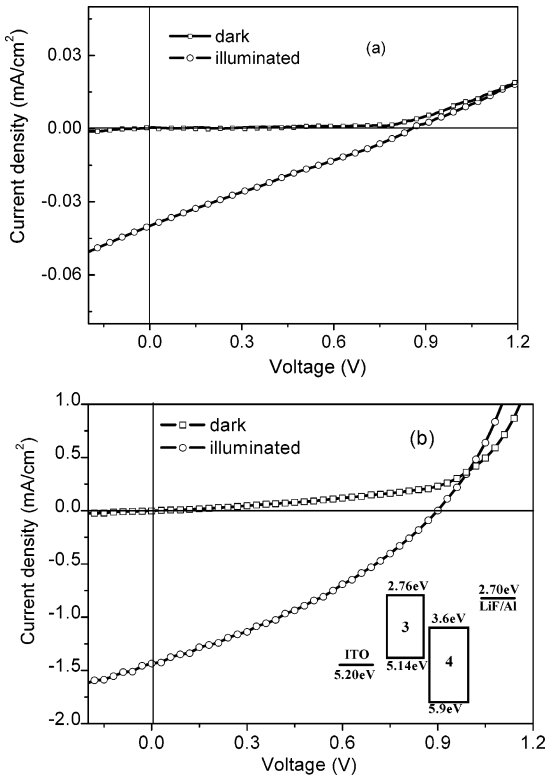

Figure 5. Current density−voltage characteristics of the OSCs with LiF/Al as cathode based on (a) the single component of TPA−DCM−TPA and (b) the blend of TPA−DCM−TPA as donor and PCBM as acceptor with a weight ratio of 1:1. Inset of (b) shows the electronic energy level diagram (**3** and **4** denote the molecules of TPA−DCM−TPA and PCBM, respectively) of the device.

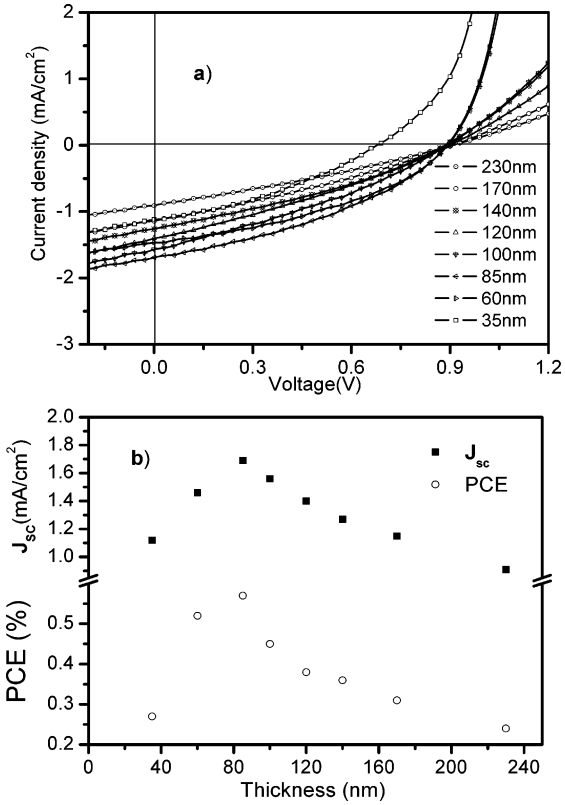

Figure 6. (a) $J-V$ curves of the OSCs with different active layer thickness and (b) dependence of PCE and J_{SC} on the active layer thickness of the OSCs under the illumination of AM 1.5, 100 mW/cm^2. The device structure of the OSCs is ITO/PEDOT:PSS/TPA−DCM−TPA:PCBM (1:1 w/w)/Ba/Al.

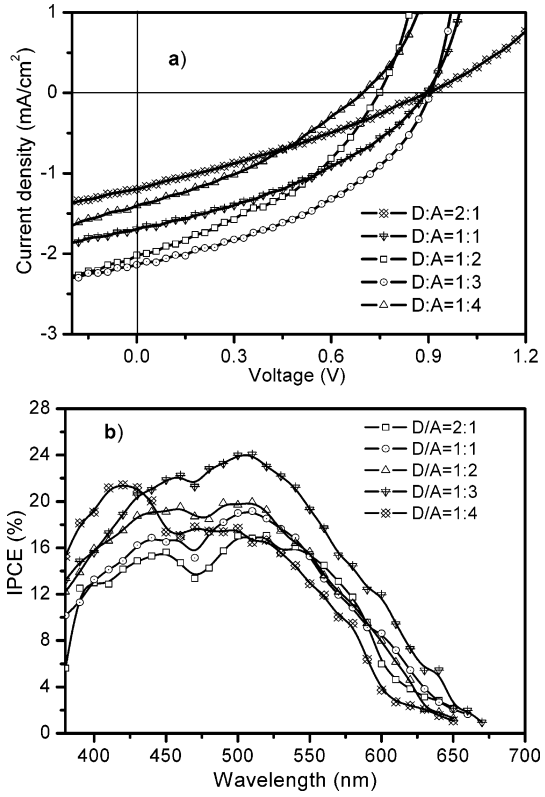

Figure 7. (a) $J-V$ curves of the OSCs with different weight ratio of TPA−DCM−TPA:PCBM (D/A) under the illumination of AM 1.5, 100 mW/cm^2 and (b) IPCE curves of the OSCs with different weight ratio of TPA−DCM−TPA:PCBM (D/A). The device structure is ITO/PEDOT:PSS/TPA−DCM−TPA:PCBM/Ba/Al.

As we expected, TPA−DCM−TPA is soluble in common organic solvents such as THF, toluene, and chlorobenzene. High-quality amorphous film can be obtained by spin-coating its solution. The AFM images of TPA−DCM−TPA film and the blend film of TPA−DCM−TPA and PCBM, as shown in Figure S1 in Supporting Information, reveal that the surface roughness is <2 nm, which displays the good film-forming ability of TPA−DCM−TPA.

The hole mobility of TPA−DCM−TPA was measured with the space-charge-limited current (SCLC) model[29,30] with a device structure of ITO/PEDOT:PSS/TPA−DCM−TPA/Au. The results were plotted as $\ln(JL^3/V^2)$ vs $(V/L)^{0.5}$, as shown in Figure S2 in Supporting Information. Hole mobility was calculated from the intercept of the corresponding lines on the axis of $\ln(JL^3/V^2)$,[30] and it was 1.19×10^{-6} cm^2/Vs.

Benefited from its donor−acceptor structure linked with conjugated bridge, TPA−DCM−TPA showed a broad absorption band covering the wavelength range from 300 to 660 nm (see Figure 2), which is favorable for the application as photovoltaic materials. In toluene solution, TPA−DCM−TPA exhibits three absorption peaks at 307, 393, and 466 nm respectively. The three absorption peaks of TPA−DCM−TPA film red-shifted to 313, 411, and 498 nm, respectively. The absorption edge of the film extends to 660 nm, from which the corresponding optical energy gap (E_g^{opt}) is calculated as 1.88 eV. The PL peak of the TPA−DCM−TPA solution in toluene was located at around 591 nm and it was red-shifted to 645 nm for the film. The PL spectrum indicates that TPA−DCM−TPA is a red-emitting organic material.

In order to determine the energy band gap as well as HOMO and LUMO energy levels, electrochemical cyclic voltammogram was measured for TPA−DCM−TPA film. As shown in Figure 3, there are a couple of reversible oxidation/re-reduction peaks in the positive potential region with the onset oxidation potential (E_{onset}^{ox}) at 0.75 V vs Ag wire and an irreversible reduction peak in the negative potential region with onset reduction potential (E_{onset}^{red}) at −1.63 V vs Ag wire. The HOMO and LUMO levels were calculated to be −5.14 and −2.76 eV, respectively, according to the equations of HOMO = $-\exp(E_{onset}^{ox} + 4.39)$ (eV) and LUMO = $-\exp(E_{onset}^{red} + 4.39)$ (eV).[31]

TPA−DCM−TPA molecule showed intramolecular light-induced charge-transfer due to its donor−acceptor structure, which was measured by the light-induced electron spin resonance (LESR) spectrum.[32] There is no ESR signal of the TPA−DCM−TPA film before illumination at room temperature. When the sample was illuminated, a light-induced ESR signal with $g = 2.0058$ was observed, as shown in Figure 4. The ESR signal intensity decreased with time after the exciting light was switched-off. This result reveals that the electron transfer occurred after light irradiation, i.e., the photoinduced electron-transfer existed in the TPA−DCM−TPA molecules. The existence of the light-induced intramolecular charge transfer indicates that TPA−DCM−TPA could be used as a photovoltaic material.

3.2. Photovoltaic Devices. The solution-processable TPA−DCM−TPA was used to fabricate the organic solar cells (OSCs) by spin-coating technique. In order to study the effect of the device composition on the performance of the OSCs, two types of OSCs were fabricated: the single-component device with TPA−DCM−TPA as the photosensitive layer and the bulk-heterojunction devices based on the blend of TPA−DCM−TPA as donor and PCBM as acceptor materials.

Figure 5 shows the current density−voltage ($J-V$) curves of the single-component and the blend (bulk-heterojunction) OSCs

TABLE 1: Photovoltaic Performance of the OSCs with Different Compositions of Active Layer under Illumination of AM 1.5, 100 mW/cm^2

composition of the active layer of OSCs	cathode materials	V_{oc} (V)	I_{sc} (mA/cm^2)	FF (%)	PCE (%)
pure TPA−DCM−TPA	LiF/Al	0.86	0.039	29	0.01
TPA−DCM−TPA:PCBM = **1:1 (w/w)**	LiF/Al	0.9	1.43	34	0.44
TPA−DCM−TPA:PCBM = **1:1 (w/w)**	Ba/Al	0.90	1.69	37.4	0.57
TPA−DCM−TPA:PCBM = **2:1 (w/w)**	Ba/Al	0.90	1.2	30	0.32
TPA−DCM−TPA:PCBM = **1:2 (w/w)**	Ba/Al	0.75	2.02	39.5	0.6
TPA−DCM−TPA:PCBM = **1:3 (w/w)**	Ba/Al	0.90	2.14	41.3	0.79
TPA−DCM−TPA:PCBM = **1:4 (w/w)**	Ba/Al	0.69	1.4	34.5	0.33

with LiF/Al as cathode. The OSC based on single-component TPA−DCM−TPA with the device structure of ITO/PEDOT:PSS/TPA−DCM−TPA)/LiF/Al (see Figure 5a) shows the photovoltaic properties with open-circuit voltage (V_{oc}) of 0.86 V, short-circuit current (J_{sc}) of 0.039 mA/cm^2, fill factor (FF) of 0.29, and power-conversion efficiency (PCE) of 0.01% under the illumination of AM1.5, 100 mW/cm^2. The obvious photovoltaic effect of the single-component device should be ascribed to the photoinduced charge separation in TPA−DCM−TPA as discussed above, but the relatively low PCE value compared with the heterojunction device should result from the inefficient charge separation and transportation; the appearance of photoluminescence in TPA−DCM−TPA film supported this view.

Figure 5b shows the energy levels and the $J-V$ curves of the bulk-heterojunction OSC based on the blend of TPA−DCM−TPA and PCBM. Both LUMO and HOMO energy levels of TPA−DCM−TPA are higher than those of PCBM by ca. 0.8 eV, which reveals that the match of the energy levels of TPA−DCM−TPA as donor and PCBM as acceptor is very good and ideal. The V_{oc}, J_{sc}, FF, and PCE of the bulk-heterojunction OSC with the device structure of ITO/PEDOT/TPA−DCM−TPA:PCBM (1:1 w/w)/LiF/Al reached 0.9 V, 1.434 mA/cm^2, 0.34, and 0.44%, respectively, under the illumination of AM1.5, 100 mW/cm^2. The efficiency of the bulk-heterojunction device is 44 times higher than that of the single-component OSC of TPA−DCM−TPA. These results indicate that the bulk-heterojunction devices are currently the most efficient structure for the solution-processable solar cells.

The cathode materials, the active layer thickness, and the weight ratio of TPA−DCM−TPA:PCBM in the active layers with the thickness of ca. 85 nm were optimized for further improving the photovoltaic performances of the heterojunction OSCs. In considering the low work function of barium, we utilized Ba as cathode in the following investigations.

Increasing the active layer thickness can increase the absorption, but it will be limited by the slow charge transportation in the active layer of the OSCs. Thus, optimization of the active layer thickness is one of the key issues to improve the efficiency of the devices. Figure 6a shows the $J-V$ curves for the devices of ITO/PEDOT/TPA−DCM−TPA:PCBM(1:1 w/w)/Ba/Al with different active layer thicknesses from 35 to 230 nm. The maximum J_{sc} and PCE of devices reached 1.69 mA/cm^2 and 0.57%, respectively, from the device with the active layer thickness of ca. 85 nm under the illumination of AM 1.5, 100 mW/cm^2. Figure 6b shows clearly the dependence of the J_{sc} and PCE on the active layer thickness. Obviously, the optimized thickness is 85 nm; thinner and thicker layers all result in lower J_{sc} and lower PCE, due to the fact that a too-thin active layer reduces the absorption of the irradiated light and a too-thick active layer affects the effective charge transportation, which is limited by the low-charge carrier mobility of the organic materials.

The effect of weight ratio of TPA−DCM−TPA:PCBM in the active layers on the photovoltaic performance was investigated for the OSCs with Ba/Al cathode. Figure 7a shows the $J-V$ characteristics of the OSCs with various weight ratios of TPA−DCM−TPA:PCBM under the illumination of AM1.5, 100 mW/cm^2. Table 1 summarized the main parameters of the devices. The J_{sc}, FF, and PCE values increase with the increase of PCBM concentration from the weight ratio of TPA−DCM−TPA:PCBM of 2:1 to that of 1:3. A higher concentration of PCBM should favor the formation of the interpenetrated networks of the PCBM acceptor, which in turn favors the effective charge separation and charge transportation. Further increase of the PCBM concentration over the weight ratio of 1:3 resulted in decrease of the J_{sc} and PCE values of the OSC, probably due to the reduction of the amount of TPA−DCM−TPA and the reduction of absorption for the same thickness of the active layers. The input photon to converted current efficiency (IPCE), as shown in Figure 7b, confirms the effect of the weight ratio of TPA−DCM−TPA:PCBM on the photovoltaic performance of the OSC devices. The optimized weight ratio of TPA−DCM−TPA:PCBM is 1:3. The V_{oc}, J_{sc}, FF, and PCE of the bulk heterojunction OSC based on the blend of TPA−DCM−TPA and PCBM (1:3 w/w) reached 0.9 V, 2.14 mA/cm^2, 0.413, and 0.79%, respectively, under the illumination of AM1.5, 100 mW/cm^2. The maximum quantum efficiency of the device reached 24% at 510 nm (see Figure 7b). In addition, the wavelength range and the shape of the IPCE curves are coincident well with the absorption spectrum of the blend film (see Figure S3, Supporting Information), which indicates that the visible absorption of TPA−DCM−TPA did make a contribution to the photovoltaic energy conversion.

4. Conclusion

A solution processable organic conjugated molecule with D−A structure and triphenylamine as donor unit and malononitrile as the acceptor unit, TPA−DCM−TPA, was designed and synthesized for the application in organic solar cells (OSCs). TPA−DCM−TPA film showed a broad absorption band covering the wavelength range of 350−650 nm. The bulk-heterojunction OSCs with TPA−DCM−TPA as donor and PCBM as acceptor materials were fabricated by spin-coating their chlorobenzene solutions. The cathode material, the weight ratio of TPA−DCM−TPA:PCBM, and the thickness of the active layer were optimized to be Ba/Al cathode, 1:3 weight ratio, and ca. 85 nm thickness, respectively. The open-circuit voltage, short-circuit current, and power-conversion efficiency of the optimized OSC reached 0.9 V, 2.14 mA/cm^2, and 0.79%, respectively, under the illumination of AM1.5, 100 mW /cm^2. The efficiency of 0.79% is among the highest values for the OSCs based on the solution processable organic small molecules. The results indicate that the triphenylamine-containing molecules could be promising organic photovoltaic materials by careful molecular design with a combination of suitable electron-deficient units.

Acknowledgment. This work was supported by the Ministry of Science and Technology of China (973 project, Nos.

2002CB613404 and 2002CB613401) and the National Natural Science Foundation of China (Nos. 20474069, 20421101, 20574078, 50503024, and 50633050).

Supporting Information Available: Supporting Information includes AFM images, current−voltage data, and UV−vis absorption spectra. This material is available free of charge via the Internet at http://pubs.acs.org.

References and Notes

(1) Hoppe, H.; Sariciftci, N. S. *J. Mater. Res.* **2004**, *19*, 1924.
(2) Winder, C.; Sariciftci, N. S. *J. Mater. Chem.* **2004**, *14*, 1077.
(3) Janssen, R. A. J.; Hummelen, J. C.; Saricifti, N. S. *MRS Bull.* **2005**, *30*, 33.
(4) Coakly, K. M.; McGehee, M. D. *Chem. Mater.* **2004**, *16*, 4533.
(5) Spanggaard, H.; Krebs, F. C.; *Sol. Energy Mater. Sol. Cells* **2004**, *83*, 125.
(6) Peumans, P.; Yakimov, A.; Forrest, S. R. *J. Appl. Phys.* **2003**, *93*, 3693.
(7) Hou, J. H.; Tan, Z. A.; Yan, Y.; He, Y. J.; Yang, C. H.; Li, Y. F. *J. Am. Chem. Soc.* **2006**, *128*, 4911.
(8) Reyes-Reyes, M.; Kim, K.; Carroll, D. L. *Appl. Phys. Lett.* **2005**, *87*, 083506.
(9) Ma, W. L.; Yang, C. Y.; Gong, X.; Lee, K.; Heeger, A. J. *Adv. Funct. Mater.* **2005**, *15*, 1617.
(10) Xue, J. G.; Rand, B. P.; Uchida, S.; Forrest, S. R. *Adv. Mater.* **2005**, *17*, 66.
(11) Forrest, S. R. *MRS Bull.* **2005**, *30*, 28.
(12) Shaheen, S. E.; Radspinner, R.; Peyghambarian, N.; Jabbour, G. E. *Appl. Phys. Lett.* **2001**, *79*, 2996.
(13) Brabec, C. J.; Hauch, J. A.; Schilinsky, P.; Waldauf, C. *MRS Bull.* **2005**, *30*, 50.
(14) Brabec, C. J.; Padinger, F.; Hummelen, J. C.; Janssen, R. A. J.; Sariciftci, N. S. *Synth. Met.* **1999**, *102*, 861.
(15) Salzman, R. F.; Xue, J. G.; Rand, B. P.; Alexander, A.; Thompson, M. E.; Forrest, S. R. *Org. Electron.* **2005**, *6*, 242.
(16) Goh, C.; Kline, R. J.; McGehee, M. D.; Kadnikova, E. N.; Frechet, J. M. J. *Appl. Phys. Lett.* **2005**, *86*, 122110.
(17) Shirota, Y. *J. Mater. Chem.* **2005**, *15*, 75.
(18) Shirota, Y. *J. Mater. Chem.* **2000**, *10*, 1.
(19) Giebeler, C.; Antoniadis, H.; Bradley, D. D. C.; Shirota, Y. *Appl. Phys. Lett.* **1998**, *72*, 2448.
(20) Roncali, J. *Chem. Rev.* **1997**, *97*, 173.
(21) Blanchard, P.; Verlhac, P.; Michaux, L.; Frère, P.; Roncali, J. *Chem.−Eur. J.* **2006**, *12*, 1244.
(22) Roncali, J. *Chem. Soc. Rev.* **2005**, *34*, 483.
(23) Roquet, S.; Cravino, A.; Leriche, P.; Alévěque, O.; Frère, P.; Roncali, J. *J. Am. Chem. Soc.* **2006**, *128*, 3459.
(24) Cremer, J.; Pauerle, B. *J. Mater. Chem.* **2006**, *16*, 874.
(25) He, C.; He, Q. G.; He, Y. J.; Li, Y. F.; Bai, F. L.; Yang, C. H.; Ding, Y. Q.;. Wang, L. X; Ye, J. P. *Sol. Energy Mater. Sol. Cells* **2006**, *90*, 1815.
(26) Sun, X. B.; Zhou, Y. H.; Wu, W. C.; Liu, Y. Q.; Tian, W. J.; Yu, G.; Qiu, W. F.; Chen, S. Y.; Zhu, D. B. *J. Phys. Chem. B* **2006**, *110*, 7702.
(27) Peng, Q.; Lu, Z. Y.; Huang, Y.; Xie, M. G.; Han, S. H.; Peng, J. B.; Cao, Y. *Macromolecules* **2004**, *37*, 260.
(28) Wenseleers, W.; Stellacci, F.; Meyer-Friedrichsen, T.; Mangel, T.; Bauer, C. A.; Pond, S. J. K.; Marder, S. R.; Perry, J. W. *J. Phys. Chem. B* **2002**, *106*, 6853.
(29) Chirvase, D. C.; Knipper, Z.; Parisi, M. J.; Dyakonov, V.; Hummelen, J. C. *Phys. Rev. B* **2004**, *70*, 235207.
(30) Malliaras, G. G.; Salem, J. R.; Brock, P. J.; Scott, C. *Phys. Rev. B* **1998**, *58*, 13411.
(31) Li, Y. F.; Cao, Y.; Gao, J.; Wang, D. L.; Yu, G.; Heeger, A. J. *Synth. Met.* **1999**, *99*, 243.
(32) Brabec, C. J.; Dyakonov, V.; Parisi, J.; Sariciftci, N. S. *Organic Photovoltaics Concepts and Realization*; Springer: Berlin, 2003.